A combined molecular dynamics and Monte Carlo study of the approach towards phase separation in colloid–polymer mixtures

2010 J. Phys.: Condens. Matter 22 104120

(http://iopscience.iop.org/0953-8984/22/10/104120)

J. Phys.: Condens. Matter **22** (2010) 104120 (11pp) doi:10.1088/0953-8984/22/10/104120

A combined molecular dynamics and Monte Carlo study of the approach towards phase separation in colloid–polymer mixtures

Jochen Zausch[1,2], **Jürgen Horbach**[3], **Peter Virnau**[1] and **Kurt Binder**[1]

[1] Institut für Physik, Johannes Gutenberg-Universität Mainz, Staudinger Weg 7, D-55099 Mainz, Germany
[2] Fraunhofer Institut für Techno- und Wirtschaftsmathematik (ITWM), Fraunhofer-Platz 1, D-67663 Kaiserslautern, Germany
[3] Institut für Materialphysik im Weltraum, Deutsches Zentrum für Luft- und Raumfahrt (DLR), D-51170 Köln, Germany

E-mail: juergen.horbach@dlr.de and kurt.binder@uni-mainz.de

Received 5 October 2009, in final form 30 November 2009
Published 23 February 2010
Online at stacks.iop.org/JPhysCM/22/104120

Abstract
A coarse-grained model for colloid–polymer mixtures is investigated where both colloids and polymer coils are represented as point-like particles interacting with spherically symmetric effective potentials. Colloid–colloid and colloid–polymer interactions are described by Weeks–Chandler–Andersen potentials, while the polymer–polymer interaction is very soft, of strength $k_BT/2$ for maximum polymer–polymer overlap. This model can be efficiently simulated both by Monte Carlo and molecular dynamics methods, and its phase diagram closely resembles that of the well-known Asakura–Oosawa model. The static and dynamic properties of the model are presented for systems at critical colloid density, varying the polymer density in the one-phase region. Applying Lees-Edwards boundary conditions, colloid–polymer mixtures exposed to shear deformation are considered, and the resulting anisotropy of correlations is studied. Whereas for the considered shear rate, $\dot{\gamma} = 0.1$, radial distribution functions and static structure factors indicate only small structural changes under shear, an appropriate projection of these correlation functions onto spherical harmonics is presented that allows us to directly quantify the structural anisotropies. However, the considered shear rate is probably not high enough to see anisotropies in static structure factors at small wavenumbers that have been predicted by Onuki and Kawasaki (1979 *Ann. Phys.* **121** 456) for the critical behavior of systems under shear. The anomalous dependence of the polymer's self-diffusion constant on polymer density is referred to the clustering of the colloid particles when approaching the critical point.

1. Introduction

Colloid–polymer mixtures exhibit a phase behavior where both liquid–vapor-type phase separation and liquid–solid (crystal) transitions occur [1–3]. Since repulsive interactions among colloidal particles are tunable to a large extent [4–6], and also the depletion attraction between colloids caused by nonadsorbing polymers [7–9] can be varied widely simply by the size of the polymer coils, the interplay between structure and dynamics, on the one hand, and the effective interaction among particles, on the other hand, can be elucidated in detail, often much better than would be possible for systems formed from small molecules. A further attractive feature of these soft matter systems is the sensibility to applied external fields [5, 6]

and, last but not least, the large size of the colloidal particles (in the micrometer range) allows the direct observation of their structure and dynamics via confocal microscopy techniques (see, e.g., [10]). As a result, these systems have become model systems allowing the real-space experimental observation of statics and dynamics of capillary waves at interfaces [11], of wetting layer formation [12–14], of critical fluctuations [15], etc. Studies of non-equilibrium phenomena have also been illuminating, such as the study of phase separation kinetics [16] and shear-induced narrowing of interfacial widths [17].

For providing a detailed understanding of such cooperative phenomena in these soft matter model systems, the interplay between experiment, theory and computer simulation has been particularly fruitful (see, e.g., [4–6] for reviews). In the case of colloid–polymer mixtures, the standard theoretical model for the description of static phenomena has been the Asakura–Oosawa model [7–9]. In this model, spherical colloidal particles are simply treated as hard spheres which may neither overlap with each other nor with the polymers. On the other hand, polymers are also modeled as spheres, but they may overlap with each other at no energy cost. This model has been studied extensively both by analytical theory and simulations (see, e.g., [1, 18–22]), providing a detailed understanding of various static properties. The phase behavior in equilibrium as well as interfacial and confinement effects [21, 22] was also elucidated.

However, since, like in an ideal gas, there is no polymer–polymer interaction energy, this model is unsuitable to describe the dynamics of the system even on a simplified, coarse-grained level (the fluid in which the colloidal particles are suspended and the polymers are dissolved still does not need to be considered explicitly). Actually, if two polymer coils in a good solvent overlap, there is a nonzero interaction energy, which may be approximately described as [23–27] $U(r) = U_0 \exp[-(r/R)^2]$, with r the distance between the center of mass of the coils and R a length of the order of their gyration radius. The pre-factor U_0 is of the order of the thermal energy $k_B T$.

This fact has been our motivation to introduce [28] a variant of the Asakura–Oosawa (AO) model where polymers have such a soft interaction, and also the discontinuous hard-core colloid–colloid and colloid–polymer interactions of the AO model are replaced by continuous potentials of the Weeks–Chandler–Andersen (WCA) type [29]. The Monte Carlo study of such a continuous variant of the AO model is not straightforward, since the generalization of the cluster move allowing a very efficient simulation in the grand-canonical ensemble [30] is nontrivial [28]. This method is discussed in [28] where also the finite-size scaling analysis of such Monte Carlo 'data' [31, 32] is described.

In the present paper, we extend the study of this model [28] describing various results obtained via molecular dynamics (MD) methods [33], varying the polymer densities but choosing the colloid density precisely at the value of the critical density of the model. This critical density has been deduced from the finite-size analysis of the Monte Carlo data [28]. In particular, we present a first feasibility test of a non-equilibrium molecular dynamics (NEMD) study [33, 34] of a colloid–polymer mixture under shear (section 5).

In section 2, we recall the precise definition of the model and also present its phase diagram. Section 3 then discusses static radial distribution functions and structure factors in equilibrium. Section 4 discusses time-dependent structure factors and mean square displacement, while section 5 summarizes our conclusions.

2. Model and equilibrium phase diagram

To describe the phase behavior of colloid–polymer mixtures, one has to consider rather dense systems and the densities of colloids and polymers may vary over a wide range. In addition, the properties of polymers are strongly affected by the 'quality of the solvent' in which they are suspended [35]. Since the interactions in colloid–polymer mixtures may strongly change when one varies the densities or the properties of the solvent, the derivation of effective interaction potentials between colloids and polymers in a colloidal suspension is a nontrivial task [23–27]. In this work, we are not aiming at deriving a realistic interaction potential, but we rather follow [28] and use a generic model that captures qualitatively the features that are relevant for describing the phase behavior of colloid–polymer mixtures under shear. In our model, interactions are also optimized with respect to computational efficiency for MD methods. In particular, we wish to work with potentials of strictly finite range, i.e. the potential $U_{\alpha\beta}$ between particles of type $\alpha\beta$ = cc, cp, pp (with 'c' denoting the colloids and 'p' the polymers) should be identically zero for distances r exceeding a cutoff $r_{c,\alpha\beta}$. For the colloid–colloid and colloid–polymer interactions we hence choose the WCA potential [29]:

$$U_{\alpha\beta}(r) = 4\epsilon_{\alpha\beta}\left[\left(\frac{\sigma_{\alpha\beta}}{r}\right)^{12} - \left(\frac{\sigma_{\alpha\beta}}{r}\right)^{6} + \frac{1}{4}\right]S, \qquad (1)$$

where $\epsilon_{\alpha\beta}$ controls the strength and $\sigma_{\alpha\beta}$ the range of the potential. The cutoff is set to $r_{c,\alpha\beta} = 2^{1/6}\sigma_{\alpha\beta}$. Since we require strict energy conservation for MD in the microcanonical ensemble, not only $U_{\alpha\beta}(r)$ has to be smooth at $r = r_{c,\alpha\beta}$ but also the forces need to be continuous everywhere. Therefore, we use a smoothing function S, given by

$$S = \frac{(r - r_{c,\alpha\beta})^4}{h^4 + (r - r_{c,\alpha\beta})^4} \qquad (2)$$

with $h = 10^{-2}\sigma_{\alpha\beta}$. In order to be able to compare with previous work on the ordinary AO model [20–22, 30] a size ratio $q = \sigma_{pp}/\sigma_{cc} = 0.8$ between polymers and colloids is chosen. Furthermore, we set $\epsilon_{cc} = \epsilon_{cp}$ and

$$\sigma_{cp} = (\sigma_{cc} + \sigma_{pp})/2 = 0.9\sigma_{cc}. \qquad (3)$$

In the following, units are given by $\sigma_{cc} = 1$, $\epsilon_{cc} = 1$ and $k_B T = 1$. For the soft polymer–polymer interaction potential, we choose

$$U_{pp}(r) = 8\epsilon_{pp}\left[1 - 10\left(\frac{r}{r_{c,pp}}\right)^3 + 15\left(\frac{r}{r_{c,pp}}\right)^4 - 6\left(\frac{r}{r_{c,pp}}\right)^5\right] \qquad (4)$$

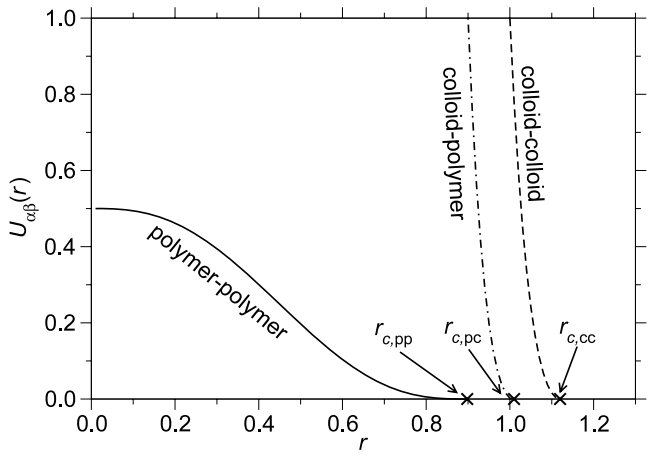

Figure 1. Potentials $U_{\alpha\beta}(r)$ describing the polymer–polymer, colloid–polymer and colloid–colloid interactions as a function of distance r. Asterisks highlight the cutoff distances, as indicated. Note that energies are measured in units of $\epsilon_{cc} = \epsilon_{cp} = k_B T = 1$.

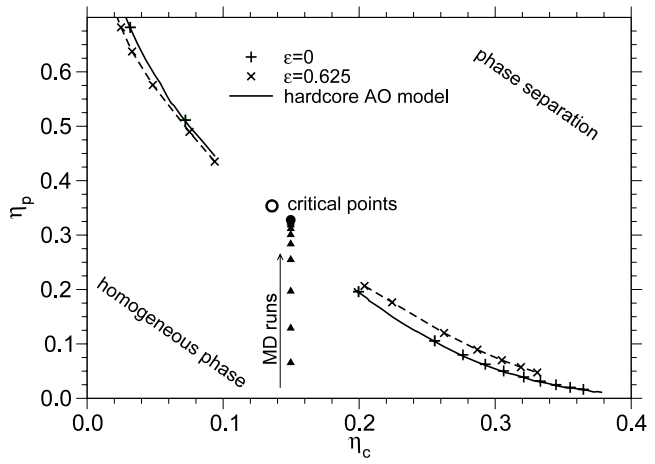

Figure 2. Phase diagrams of three models describing colloid–polymer mixtures, in the plane of variables η_p (polymer packing fraction) and η_c (colloid packing fraction) as defined in equation (7). The original AO model (studied in [20, 30]) is shown by a full curve, with its critical point by an open circle. A soft variant of this model (using WCA potentials as defined in equations (1) and (2) but still strictly non-interacting polymers, i.e. $\epsilon_{pp} = 0$) is shown by standing crosses, while the broken curve and crosses (×) denote the model studied in the present paper, where equation (4) with $\epsilon_{pp} = 0.0625$ is used. The full dot shows the critical point of the latter model. The triangles indicate state points at which MD runs in equilibrium (without shear) were performed. Reprinted with permission from [28]. Copyright 2009 by the American Institute of Physics.

with $\epsilon_{pp} = 0.0625$. Figure 1 displays all three potentials as a function of distance [28]. Note that the potential function in equation (4) has a similar shape as a cosine function; this function provides that both the force and the potential vanish at $r_{c,pp}$, as required.

In the ordinary AO model, the phase behavior is often discussed using the packing fractions η_c, η_p of colloids and polymers as variables rather than the densities ρ_c and ρ_p:

$$\eta_c = \rho_c V_c, \qquad \eta_p = \rho_p V_p, \tag{5}$$

where V_c and V_p are the volumes occupied by a colloid and polymer, respectively ($V_c = \pi d_{cc}^3/6$ and $V_p = \pi d_{pp}^3/6$, where d_{cc} and d_{pp} denote the diameter of the spheres representing colloids and polymers, respectively). In order to be able to compare the present continuous variant of the AO model to its original, discontinuous version, we define an effective diameter of colloids and polymers, following Barker and Henderson [37]:

$$d_{\alpha\beta} = \int_0^{\sigma_{\alpha\beta}} (1 - \exp[-U_{\alpha\beta}(r)/k_B T])\, \mathrm{d}r, \tag{6}$$

which yields $d_{cc} = 1.015\,57\sigma_{cc}$ and $d_{cp} = 0.9 d_{cc}$. Inserting $d_{pp} = 0.8 d_{cc}$, we finally obtain the following conversion formulae between densities and effective packing fractions:

$$\eta_c = 0.548\,44\sigma_{cc}^3 \rho_c, \qquad \eta_p = 0.280\,80\sigma_{cc}^3 \rho_p. \tag{7}$$

While for the critical point of vapor–liquid type demixing one finds in the case of the ordinary AO model for $q = 0.8$ that [30]

$$\eta_{c,crit} = 0.134, \qquad \eta_{p,crit} = 0.356, \tag{8}$$

in the case of soft polymer–polymer repulsion (equation (4)) the critical point is shifted to somewhat higher colloid and lower polymer packing fraction:

$$\eta_{c,crit} = 0.150, \qquad \eta_{p,crit} = 0.328. \tag{9}$$

In addition, there occurs a slight enhancement of miscibility on the colloid-rich side and a slight depression of the miscibility gap on the polymer-rich side of the phase diagram in the (η_p, η_c) plane (figure 2). The increase of the polymer density at high colloid packing fractions over that of the hard-core AO model follows the trend seen in experiments of colloid–polymer mixtures (see [36] and references therein). Note that the change of the phase diagram in comparison with the standard AO model is practically only due to the repulsive polymer–polymer interactions: if one uses equations (1) and (2), but sets $\epsilon_{pp} = 0$ in equation (4), the phase diagram is almost indistinguishable from the standard AO model (figure 2). Note that both the critical point and the coexistence curve separating the one-phase region from the region where phase separation occurs were found by MC methods [28].

In figure 2 the state points at which microcanonical MD runs were performed are indicated as well. In all cases, particles were put into a cubic simulation box with linear size $L = 27.0$, using periodic boundary conditions in the three spatial directions (recall that the unit of length is $\sigma_{cc} = 1$). Fixing the number of colloids at $N_c = 5373$, we thus realize that the system is always at a packing fraction η_c equal to the critical packing fraction, $\eta_c = \eta_{c,crit} = 0.15$. Then, the number of polymers varies from zero to $N_p = 22\,734$. The MD runs were carried out with the velocity Verlet algorithm [33] and a time step $\delta t = 0.0005(\sigma_{cc} m_c/\epsilon_{cc})^{1/2}$. For the sake of efficiency of the algorithm, the masses of colloids and polymers are taken to be equal, $m_c = m_p = 1$ (thus specifying the units of time).

When one uses MD to compute dynamic correlation functions and transport phenomena in thermal equilibrium, it

is desirable to work strictly in the microcanonical ensemble, since it is well known that the use of 'thermostats' for MD simulations may affect the dynamic correlations in an uncontrolled and undesirable way [33, 38, 39]. In this case, however, we need to generate initial states which represent system configurations in equilibrium for the desired conditions (e.g. the canonical ensemble for $k_BT = 1$).

First, we equilibrated a small system with $L = 9$, starting with a random initial configuration of colloids with $N_c/27$ and $N_p/27$, and ran the system at $k_BT = 1$ for 20×10^6 MD time steps with a simple velocity rescaling according to the Maxwell–Boltzmann distribution. Then, the system was enlarged from $L = 9$ to 27 by replicating it three times in all spatial directions. Periodic boundary conditions were applied for $L = 27$ only and equilibration continued with the same 'Maxwell–Boltzmann thermostat' as before for another 2×10^6 time steps. During this period, the initial periodicity with $L = 9$ is quickly lost. The production runs for static averages are done without applying any thermostat. First, 5×10^6 time steps are performed during which (at eight different times) statistically independent configurations are stored. These serve as initial configurations for eight independent simulation runs, each with 5×10^6 time steps, for the computation of static averages. During each run, 500 configurations are analyzed in regular intervals. Thus, averages are taken over 4000 statistically independent configurations.

3. Static correlations

Colloid–polymer mixtures exhibit a demixing transition, associated with the coexistence of a colloid-rich (polymer-poor) phase with a colloid-poor (polymer-rich) phase. This transition occurs because the depletion of polymer particles leads to an effective attraction between the colloids. This depletion effect can be incorporated into a one-component AO model where the polymer's degrees of freedom are expressed by an attractive part in the interaction potential between the colloids. In the latter case, the demixing transition is an ordinary liquid–gas transition. Although the one-component AO model is appealing due to its simplicity, it leaves out interesting features of real colloid–polymer mixtures, such as correlations between the polymers close to the critical point. In the modified AO model, presented here, the soft interactions between the polymers lead to a weak short-range ordering between the polymers and to a modification of the phase diagram, as indicated by figure 2. In this section, we discuss the behavior of static density correlation functions and the susceptibility when approaching the critical point from the one-phase region.

The basic quantities for the following analysis are the pair correlation functions between particles of type α and $\beta(\alpha, \beta \in \{c, p\})$ [29]:

$$G_{\alpha\beta}(\vec{r}) = \frac{L^3}{N_\alpha N_\beta}\left\langle \sum_{i=1}^{N_\alpha} \sum_{j(\neq i)}^{N_\beta} \delta(\vec{r}_i - \vec{r}_j - \vec{r})\right\rangle. \quad (10)$$

In equilibrium, the fluid is isotropic and hence it makes sense to integrate over angles and consider only the partial radial distribution functions $g_{\alpha\beta}(r)$:

$$g_{\alpha\beta}(r) = \frac{L^3}{4\pi r^2 N_\alpha N_\beta}\left\langle \sum_{i=1}^{N_\alpha} \sum_{j=1}^{N_\beta} \delta(|\vec{r}_i - \vec{r}_j| - r)\right\rangle. \quad (11)$$

When shear is applied (section 5), directions parallel and perpendicular to the flow are no longer equivalent and we need to consider the resulting anisotropy of $G_{\alpha\beta}(\vec{r})$.

Particularly important are the Fourier transforms of these correlations, since they are accessible experimentally via scattering experiments, as is well known [29]. The partial structure factors are defined by

$$S_{\alpha\beta}(\vec{q}) = \frac{1}{N}\left\langle \sum_{i=1}^{N_\alpha} \sum_{j=1}^{N_\beta} \exp[-\mathrm{i}\vec{q} \cdot (\vec{r}_i^{\,\alpha} - \vec{r}_j^{\,\beta})]\right\rangle, \quad (12)$$

which can also be rewritten as $[c_\alpha \equiv N_\alpha/(N_\alpha + N_\beta) = N_\alpha/N]$:

$$S_{\alpha\beta}(\vec{q}) = c_\alpha \delta_{\alpha\beta} + c_\alpha c_\beta \frac{N}{L^3} \int G_{\alpha\beta}(\vec{r}) \exp[-i\vec{q} \cdot \vec{r}]\, \mathrm{d}^3\vec{r}. \quad (13)$$

In equilibrium, $S_{\alpha\beta}$ does not depend on the direction of $\vec{q}$, of course, but again we will find an anisotropy of $S_{\alpha\beta}(\vec{q})$ in the case of the mixture under shear (section 5). Note that equations (10)–(13) are valid definitions for the case of steady-state shear as well.

Figures 3 and 4 show the partial radial distribution functions and the corresponding static partial structure factors, respectively. The partial radial distribution function $g_{cc}(r)$ pertaining to the colloids exhibits, for small polymer packing fraction η_p, the behavior typical for moderately dense fluids: $g_{cc}(r)$ is strictly zero for smaller r where the repulsive interaction, equation (1), prevails, while at $r \approx 1.25$ a rather sharp peak due to the nearest-neighbor shell occurs. The typical further oscillations are rather weak and $g_{cc}(r)$ rapidly tends towards unity, as expected, since η_c is still rather small. However, when η_p increases, one sees, for r up to about $r \approx 5$, a slowly decaying tail where $g_{cc}(r) > 1$ develops: this is the hallmark of the incumbent growth of long-range density correlations. These density correlations are more distinctly seen in the partial structure factor $S_{cc}(q)$, figure 4(a), where at small q a peak grows that represents the critical scattering. The oscillations at large q in figure 4(a) are not much affected by the increase of η_p, as far as their location is concerned (the intensity of $S(q)$ for large q decreases strongly with increasing η_p, since the denominator $N = N_c + N_p$ in equation (12) increases when η_p increases, of course).

The radial distribution function $g_{cp}(r)$ referring to colloid–polymer pairs, figure 3(b), is also essentially zero for small r and exhibits a rather sharp but not very high peak at about the same position as the function $g_{cc}(r)$, but the minimum that follows is more pronounced than the first minimum of $g_{cc}(r)$. When η_p increases, a slowly decaying tail at larger r also develops, but now $g_{cp}(r) < 1$ in this region. As a consequence, the resulting structure factor $S_{cp}(q)$, figure 4(b), develops at small q a pronounced anomaly but there $S_{cp}(q) < 0$.

In the polymer–polymer radial distribution function $g_{pp}(r)$ (figure 3(c)) and the associated structure factor $S_{pp}(q)$

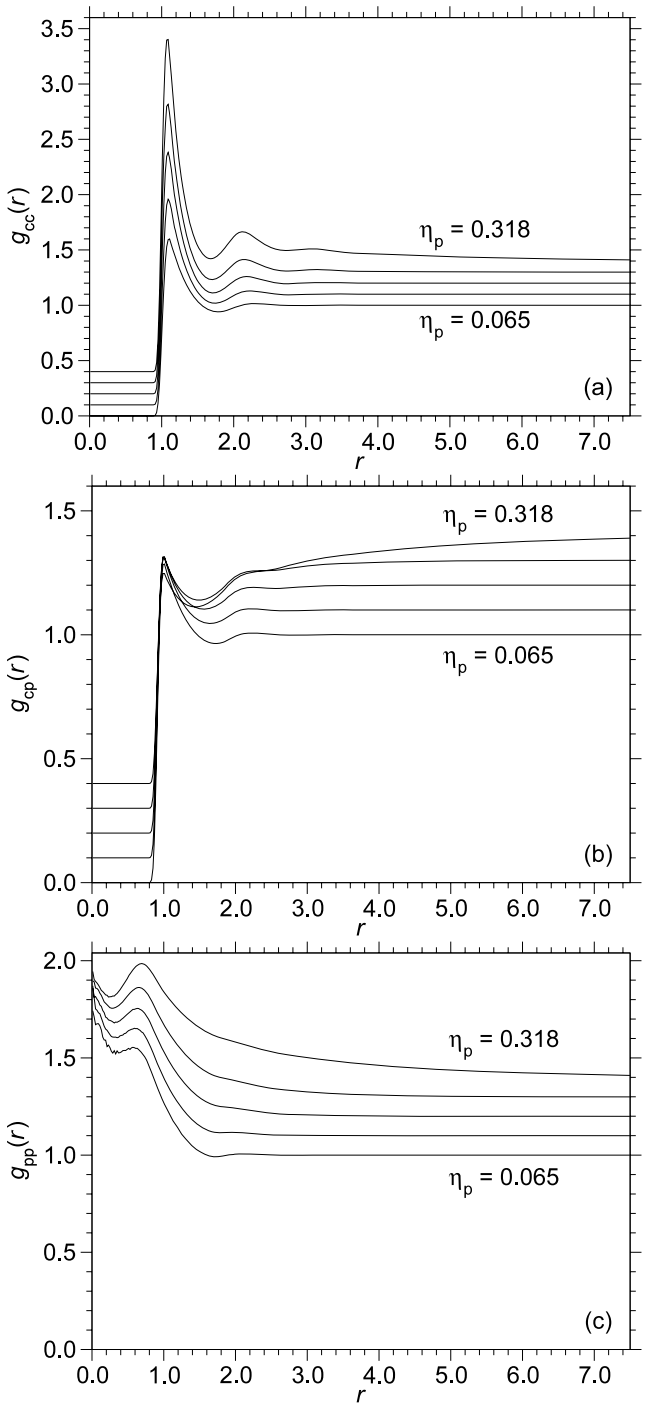

Figure 3. Partial radial distribution functions $g_{cc}(r)$ of colloid–colloid pairs (a), $g_{cp}(r)$ of colloid–polymer pairs (b) and $g_{pp}(r)$ referring to polymer–polymer pairs (c), plotted as a function of r, for a system with $L = 27$ and $N_c = 5373$. The curves refer to a variation of the polymer packing fraction $\eta_p = 0.065$, 0.129, 0.197, 0.255 and 0.318 (from bottom to top). Note that the curves are shifted with respect to each other in steps of 0.1 with respect to the y axis.

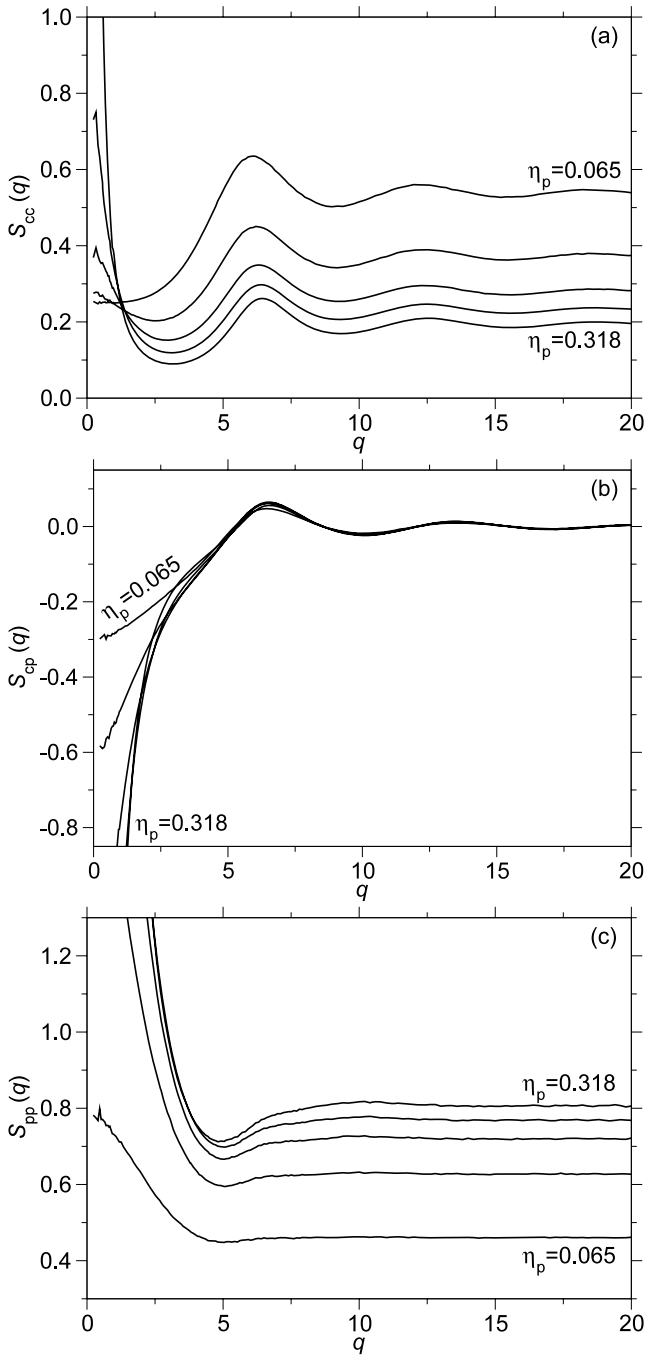

Figure 4. Partial structure factors $S_{cc}(q)$ of colloid–colloid pairs (a), $S_{cp}(q)$ of colloid–polymer pairs (b) and $S_{pp}(q)$ of polymer–polymer pairs (c), plotted as a function of wavenumber q. As in figure 3, the colloid packing fraction is $\eta_c = \eta_{c,crit} = 0.15$ in a box of linear dimension $L = 27$. The curves refer to a variation of η_p from $\eta_p = 0.065$ to 0.318 (cf figure 3), as indicated in the figure.

(figure 4(c)) one finds again the signatures of a growing range of density correlations of the polymers when η_p increases. Since the polymers can overlap with little energy cost, $g_{pp}(r)$ at small r is nonzero (and even distinctly larger than unity), and also $S_{pp}(q)$ has a maximum at $q = 0$ for all values of η_p. A particularly interesting feature is the non-monotonic decay of $g_{pp}(r)$ with r for small r (figure 3(c)). For the standard AO model, $g_{pp}(r)$ has a broad maximum at $r = 0$ (the entropic attraction between polymers caused by the colloids favors the possibility that polymers sit on top of each other) which decays to one for large r monotonically. In

the present model, the competition of this depletion attraction with the repulsion described by equation (4) causes this more complicated structure.

As discussed already in [28], various linear combinations can be formed out of $S_{cc}(q)$, $S_{cp}(q)$ and $S_{pp}(q)$, which at small q can all be analyzed according to an Ornstein–Zernike behavior:

$$S_{\alpha\beta}(q) = k_B T \chi_{\alpha\beta}/(1 + q^2\xi_{\alpha\beta}^2), \tag{14}$$

where $\chi_{\alpha\beta}$ is a 'susceptibility' and $\xi_{\alpha\beta}$ the correlation length. It was found that both $\chi_{\alpha\beta}$ and $\xi_{\alpha\beta}$ increase when η_p approaches the critical point $\eta_{p,crit}$. While $\chi_{\alpha\beta}$ depends on the type of linear combination that is considered, $\xi_{\alpha\beta}$ does not, i.e. there occurs a unique correlation length in the system [28].

To provide a background for our study of the structure factor in the presence of shear, we recall a few central points of the analysis of [28]. First of all, we note that for a binary (A, B) mixture the partial structure factors $S_{AA}(q)$, $S_{AB}(q)$ and $S_{BB}(q)$ can be used to study structure factors $S_{NN}(q)$, describing the fluctuations of total density and $S_{CC}(q)$ [40] describing the fluctuation of the relative concentration:

$$S_{NN}(q) = S_{AA}(q) + 2S_{AB}(q) + S_{BB}(q), \tag{15}$$

$$S_{CC}(q) = x_B^2 S_{AA}(q) + x_A^2 S_{BB}(q) - 2x_A x_B S_{AA}(q), \tag{16}$$

where $x_A = N_A/(N_A + N_B)$ and $x_B = N_B/(N_A + N_B)$. Also a structure factor $S_{NC}(q)$ describing the coupling between density and concentration fluctuations can be defined [40] and studied. Furthermore one can interpret the structure factors $S_{AA}(q)$, $S_{AB}(q) = S_{BA}(q)$ and $S_{BB}(q)$ as elements of a (2×2) matrix and determine the eigenvalues $S_+(q)$, $S_-(q)$ of this matrix [28]. Figure 5 shows log–log plots of the susceptibilities $k_B T\chi$ and correlation length ξ plotted as a function of the reduced distance $\epsilon \equiv 1 - \eta_p/\eta_{p,crit}$ (remember that $\eta_{p,crit}$ is not an adjustable parameter here). The possible power law behavior $\epsilon^{-\gamma}$ or $\epsilon^{-\gamma_r}$, where $\gamma_r = \gamma/(1-\alpha)$ [41], and $\epsilon^{-\nu}$ or $\epsilon^{-\nu_r}$, where $\nu_r = \nu/(1-\alpha)$, α, γ, ν being the standard Ising model critical exponents ($\nu \approx 0.63$ with $3\nu = 2 - \alpha$) [42], are also indicated. Of course, in order to unambiguously extract such critical exponents, one needs data in the range $10^{-3} \leqslant \epsilon \leqslant 10^{-1}$, which would require considerably larger computational effort than was presently possible.

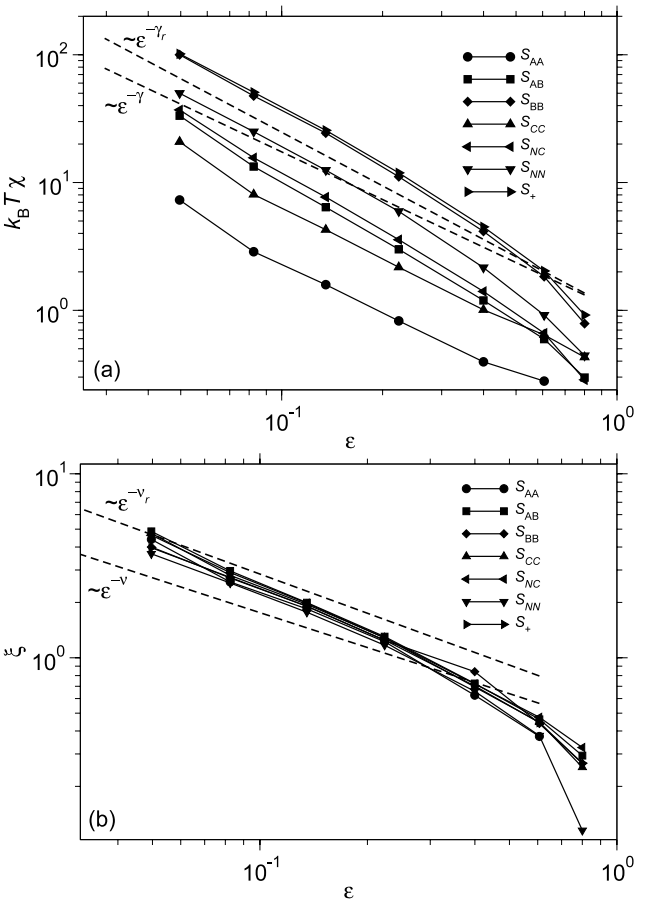

Figure 5. Log–log plots of (a) $k_B T\chi$ and (b) ξ versus $\epsilon = 1 - \eta_p/\eta_{p,crit}$ from MD simulations. The symbols (connected by lines to guide the eye) describe the various structure factors $S_{\alpha\beta}(q)$ that were analyzed in terms of equation (14), as indicated in the figure. The broken straight lines indicate the possible asymptotic power laws, with Fisher [41] 'renormalization' (γ_r, ν_r) and without it (γ, ν). Although the simulation data indicate the onset of critical divergences, they are not close enough to the critical point to distinguish between these possibilities.

4. Time-displaced correlations in thermal equilibrium

From the MD runs one obtains straightforwardly the time-displaced mean square displacements of the two types (A = colloids, B = polymers) of particles:

$$g_\alpha(t) = \frac{1}{N_\alpha}\langle[\vec{r}_i(t) - \vec{r}_i(0)]^2\rangle, \qquad \alpha \in A, B, \tag{17}$$

where the sum is extended over particles of α kind only, and the thermal average $\langle\cdots\rangle$ is realized by an average over 16 statistically independent time origins. Also other quantities (intermediate structure functions and a mean square displacement related to the interdiffusion of particles) have been obtained [28] but shall not be discussed here again, since here we wish to discuss only those properties which we have also studied when the system is exposed to shear (section 5).

The mean square displacements, equation (17), are of particular interest since the behavior at large times t immediately yields information on the self-diffusion constant D_α of the particles, via the Einstein relation

$$g_\alpha(t) = 6D_\alpha t, \qquad t \to \infty. \tag{18}$$

For times t less than the time unit $\tau = (\sigma_{cc}^2 m_c/\epsilon_{cc})^{1/2} = 1$ one observes a 'ballistic' regime $g_\alpha(t) \propto t^2$ as in free flight motion, since for very small displacements the interactions among the particles are hardly felt; for t of the order of τ there is a slow crossover from this ballistic regime to the diffusive behavior described by equation (18). Of course, this ballistic regime is somewhat unphysical; in real colloidal systems there would be another diffusive regime controlled by the solvent viscosity. In order to make sure that the regime is reached where equation (18) actually holds, it is useful to calculate $dg_\alpha(t)/dt$ [28]; we have used this derivative to read off the

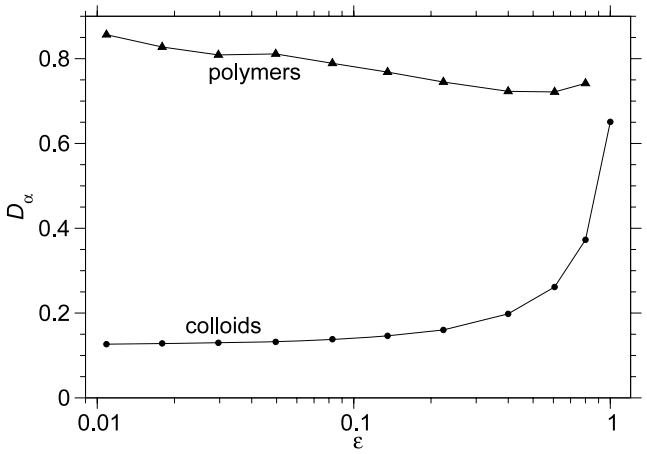

Figure 6. Self-diffusion constants D_α of colloids ($\alpha = \mathrm{c}$) and polymers ($\alpha = \mathrm{p}$) plotted versus $\epsilon = 1 - \eta_\mathrm{p}/\eta_\mathrm{p,crit}$ for colloid–polymer mixtures at the critical colloid concentration, $\eta_\mathrm{c,crit} = 0.15$.

self-diffusion constants D_α at long times. Figure 6 displays the temperature dependence of the D_α at equilibrium. While for small polymer concentration D_p and D_c are of the same order, the motion of colloids is significantly slowed down when the polymer concentration increases, but it is clear that D_p remains nonzero as $\eta_\mathrm{p} \to \eta_\mathrm{p,crit}$ and D_c also does not exhibit any visible critical singularity there. Interestingly, the polymer self-diffusion constant D_p exhibits a non-monotonic behavior with η_p: there occurs a shallow minimum at about $\epsilon \approx 0.5$, and D_p seems to get enhanced for $\epsilon \to 0$ ($\eta_\mathrm{p} \to \eta_\mathrm{p,crit}$). To our knowledge, a theoretical explanation for this effect is lacking; it means that the motion of polymers gets slightly enhanced by the critical fluctuations (where, due to the clustering of the colloids, presumably less collisions between colloids and polymers occur and hence it becomes easier for the polymers to diffuse in the polymer-rich percolating channels through the system).

5. Colloid–polymer mixtures under shear: a feasibility study

As is well known, a simulation of shear flow requires a modification of the standard periodic boundary conditions, as proposed by Lees and Edwards [43]. Defining a shear rate $\dot\gamma$ for a steady shear where the velocity field $\vec v$ is oriented along the x axis and $\partial v_x/\partial y = \dot\gamma$ via

$$\dot\gamma = v_\mathrm{s}/L, \tag{19}$$

for a simulation of $L \times L \times L$ boxes, one modifies the standard periodic boundary condition as follows: as in usual periodic boundary conditions a particle that crosses the boundary at $y = L$ or 0 is mapped back into the actual simulation box by respectively subtracting L or adding L to y such that $0 \leqslant y < L$, but in addition one subtracts or adds the actual box displacement $d = \dot\gamma t L$ to the x coordinate and subtracts/adds v_s to the velocity component v_x.

In flow and vorticity direction, i.e. x and z, the periodic boundary conditions remain unchanged. By this algorithm, when steady-state conditions are established, the upper and lower layers of the simulation box flow with velocities $v_\mathrm{s}/2$ and $-v_\mathrm{s}/2$, while the center of the simulation box is at rest. Applying a shear rate $\dot\gamma = 0.1$, we have checked [44] that no shear banding occurs, and so we observe a velocity profile which is strictly linear in the y direction.

Of course, in the motion of individual particles one has a superposition of the thermal and streaming motions, and now it is no longer possible to carry out a strictly microcanonical MD simulation, due to the entropy production (i.e. heat production) caused by the shear. Therefore, the use of suitable thermostats is mandatory to maintain a constant temperature in the system [33, 34]. The choice of a suitable thermostat for such simulations needs to be considered with great care [44]. In order not to violate local momentum conservation, thus providing a correct description of the system in the hydrodynamic limit, the choice of the dissipative particle dynamics (DPD) thermostat [45, 46] would be preferable, but it can only be used (in its standard implementation) for rather low shear rates [44]. Therefore, we used another thermostat, recently proposed by Bussi *et al* [47], which also works well for rather high shear rates although it has the disadvantage that it does not conserve momentum locally and hence is not strictly consistent with hydrodynamics. This thermostat works efficiently also if $1/\dot\gamma$ is not much, say a factor of 100–1000, larger than the typical microscopic timescale of the system, $\tau(\sigma_\mathrm{cc}^2 m_\mathrm{c}/\epsilon_\mathrm{cc})^{1/2} = 1$. As in the Berendsen thermostat [48], the Bussi thermostat uses a velocity rescaling scheme to adjust the temperature of the system, but different from the Berendsen thermostat it yields a correct description of the canonical ensemble in thermal equilibrium. In the scheme proposed by Bussi *et al* the velocities of the particles are rescaled in every time step δt by a factor α which is calculated from the following expression:

$$\alpha^2 = \mathrm{e}^{-\delta t/\tau_\mathrm{th}} + \frac{1}{2k_\mathrm{B}TK}(1 - \mathrm{e}^{-\delta t/\tau_\mathrm{th}})\left(R_1^2 + \sum_{i=2}^{3N} R_i^2\right) + 2R_1\mathrm{e}^{-\delta t/2\tau_\mathrm{th}}\sqrt{\frac{1}{2k_\mathrm{B}TK}(1 - \mathrm{e}^{-\delta t/\tau_\mathrm{th}})}. \tag{20}$$

Here, K is the instantaneous kinetic energy of the system and the R_i are independent random numbers from a Gaussian distribution with zero mean and unit variance. The parameter τ_th controls the timescale by which the thermostat responds to fluctuations of the temperature. In the present study, we have chosen the value $\tau_\mathrm{th} = 2.0$. For the considered shear rate $\dot\gamma = 0.1$, we carefully checked that a constant temperature (namely $k_\mathrm{B}T = 1$) was indeed achieved in all cases [44]. The system was run for 10^6 MD time steps of step size $\delta t = 0.005$ and, since in the beginning of the simulation the system is not yet in the steadily flowing state, only the second half of the runs was used for the data analysis.

Figure 7 shows the radial distribution functions $g_\mathrm{cc}(r)$, $g_\mathrm{cp}(r)$ and $g_\mathrm{pp}(r)$ versus r for various polymer packing fractions. Also included in the figure are their counterparts for the unsheared systems at $\eta_\mathrm{p} = 0.197$ and 0.312 (dotted lines). Whereas there are no differences between the sheared and the unsheared case at low density, at high density tiny

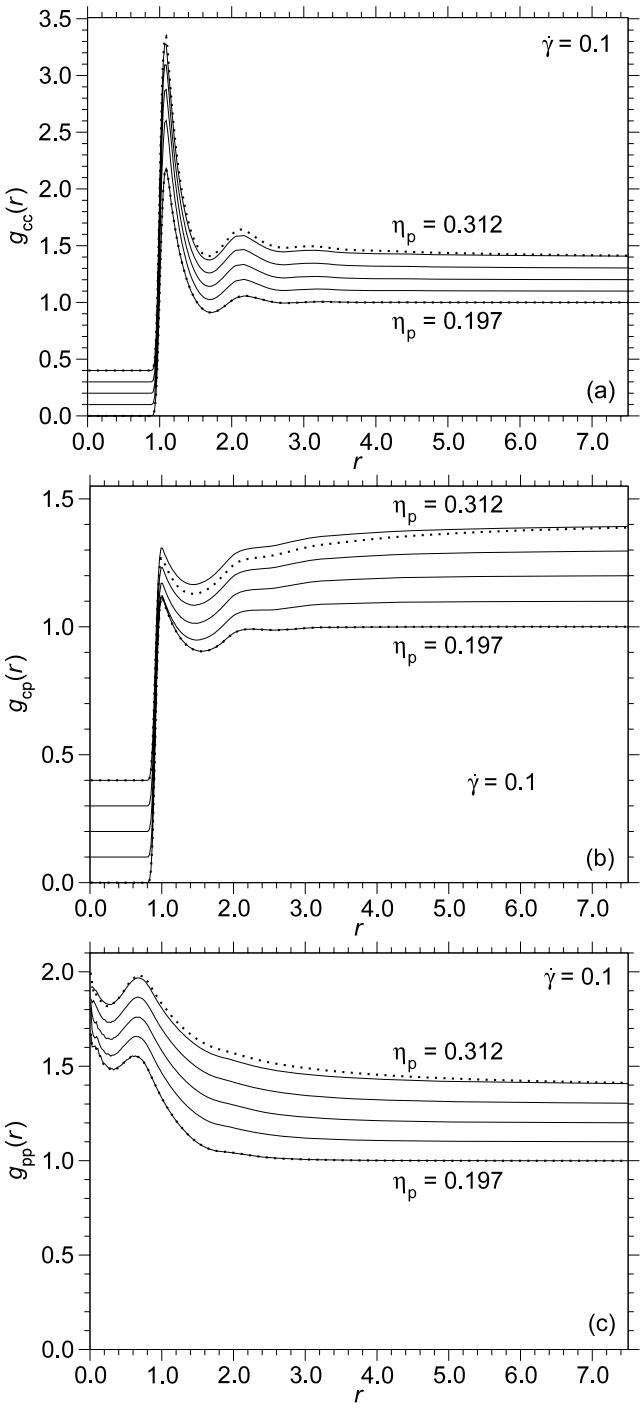

Figure 7. Partial radial distribution functions $g_{cc}(r)$ of colloid–colloid pairs (a), $g_{cp}(r)$ of colloid–polymer pairs (b) and $g_{pp}(r)$ of polymer–polymer pairs (c) plotted as a function of r for a system with $L = 27$ and $N_c = 5373$. The curves refer to a variation of the polymer packing fraction $\eta_p = 0.197$, 0.255, 0.283, 0.301 and 0.312 (from top to bottom). The shear rate $\dot\gamma = 0.1$ was used throughout. The dotted lines display $g_{\alpha\beta}(r)$ for the unsheared systems at $\eta_p = 0.197$ and 0.312. As in figure 3, the curves are shifted with respect to each other in steps of 0.1 with respect to the y axis.

differences are visible for large values of r. However, the shear-induced anisotropy becomes more apparent when one considers the expansion of the pair correlation function $G_{\alpha\beta}(\vec r)$ (equation (10)) into spherical harmonics [44, 49]:

$$G_{\alpha\beta}(\vec r) = \sum_{\ell=0}^{\infty}\sum_{m=-\ell}^{+\ell} g_{\ell m}^{(\alpha\beta)}(r) Y_{\ell m}(\Theta,\varphi). \tag{21}$$

Since $g_{00}^{(\alpha\beta)}(r)$ corresponds to the usual radial distribution function $g_{\alpha\beta}(r)$ and since the antisymmetry of the spherical harmonics implies that the coefficients with $\ell = 1$ vanish, as well as the coefficients with $\ell = 2$ if $m = 0$ or ±1, the lowest-order coefficients of interest are those of $\ell = 2$ with $m = \pm2$. Since $\{Y_{22}(\Theta,\varphi)\} = \sqrt{\frac{15}{8\pi}}\frac{xy}{r^2}$, this implies that the imaginary part of $g_{\alpha\beta,22}(r)$ is nonvanishing if $G_{\alpha\beta}(\vec r)$ is anisotropic (of course, all coefficients $g_{\ell m}^{(\alpha\beta)}(r)$ except for $g_{00}^{(\alpha\beta)}(r)$ vanish in the absence of shear since then $G_{\alpha\beta}(\vec r)$ does not display any angular dependence). We can compute this imaginary part directly from the simulation using the formula [44]

$$\mathrm{Im}\{g_{22}^{(\alpha\beta)}(r)\} = \sqrt{\frac{15}{8\pi}}\frac{L^3}{N_\alpha N_\beta} \times\left\langle\sum_{i=1}^{N_\alpha}\sum_{j(\neq i)=1}^{N_\beta}\delta(|\vec r_i^{\,\alpha}-\vec r_j^{\,\beta}|-r)\frac{(x_i^\alpha-x_j^\beta)(y_i^\alpha-y_j^\beta)}{|\vec r_i^{\,\alpha}-\vec r_j^{\,\beta}|^4}\right\rangle. \tag{22}$$

Figure 8 shows that indeed in these imaginary parts of $g_{22}^{(cc)}(r)$, $g_{22}^{(cp)}(r)$ and $g_{22}^{(pp)}(r)$ one finds considerable structure, and the range over which these imaginary parts are distinctly different from zero clearly increases with increasing polymer packing fraction. Since, according to theory [50] one must expect, however, that the critical point $(\eta_{c,crit}, \eta_{p,crit})$ gets shifted in the sheared fluid mixture relative to its location in the $(\eta_{c,crit}, \eta_{p,crit})$ plane in equilibrium, an analysis of critical behavior under shear on the basis of these data would be premature! In the equilibrium case, we had the huge advantage that the location of the critical point as well as the whole coexistence curve could be established relatively easily by Monte Carlo simulation in the grand-canonical ensemble; this advantage is lost for systems under shear. Developing new methods that would allow us to find the critical point of systems under shear that are not based on an analysis of $G_{\alpha\beta}(\vec r)$ and $S_{\alpha\beta}(\vec q)$ are beyond the scope of the present study, however.

The theory in [50] predicts a rather pronounced anisotropy of the structure factors $S_{\alpha\beta}(\vec q)$ for systems under shear, for $\eta_c = \eta_{c,crit}(\dot\gamma)$:

$$S_{\alpha\beta}^{-1}(q) = A_{\alpha\beta}(\dot\gamma)[1-\eta_p/\eta_{p,crit}(\dot\gamma)]^\gamma + B_{\alpha\beta}(\dot q)q_x^a + C_{\alpha\beta}(\dot\gamma)q^2 \tag{23}$$

where the exponent α is given by [50] $\alpha = 2/5$ and $\gamma \approx 1.23$ is the standard critical exponent of $S_{\alpha\beta}^{-1}(q = 0)$ (there should be no confusion between this exponent and the use of the symbol $\dot\gamma$ for the shear rate). Some experimental evidence for equation (23) has indeed been seen in mixtures of small molecules under shear [51]. Since in the present study only a simple nonzero shear rate was used, we do not discuss here the dependence of the critical point location and of the pre-factors $A_{\alpha\beta}$, $B_{\alpha\beta}$ and $C_{\alpha\beta}$ on shear rate further. Thus, we have also looked for possible effects of the shear on the structure factors

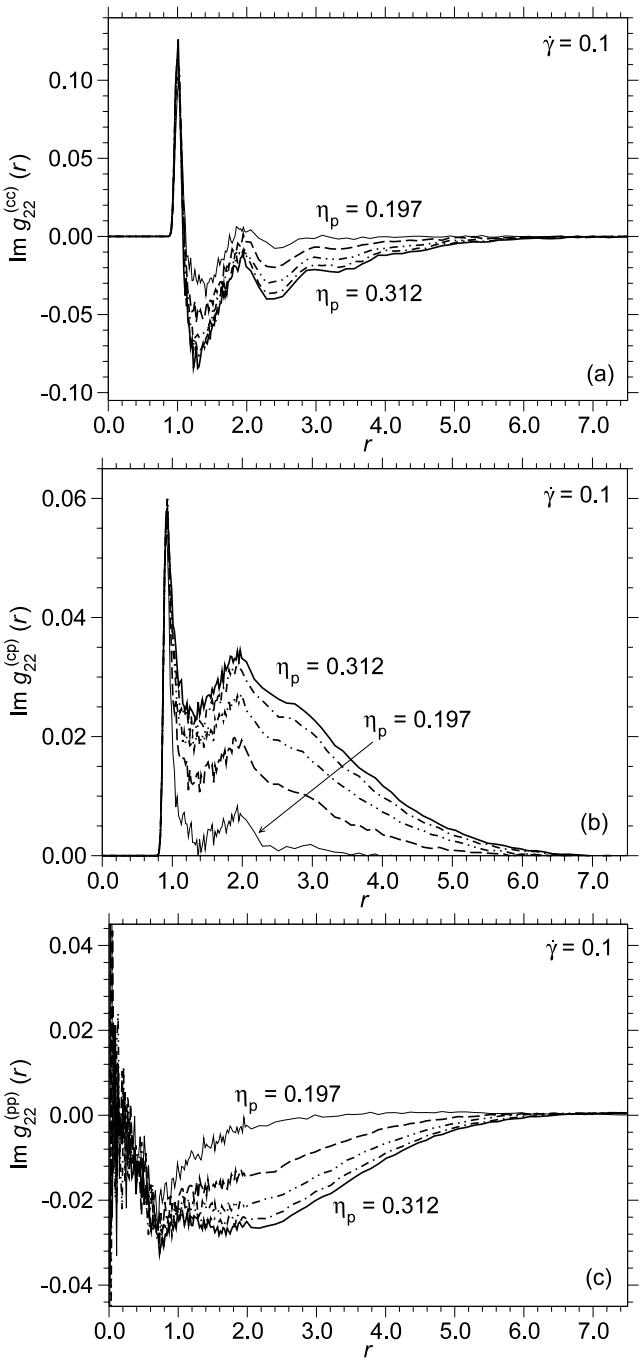

Figure 8. Imaginary parts of the distribution functions $g_{cc}^{(22)}(r)$ of colloid–colloid pairs (a), $g_{cp}^{(22)}(r)$ of colloid–polymer pairs (b) and $g_{pp}^{(22)}(r)$ of polymer–polymer pairs (c) for the same conditions as in figure 7.

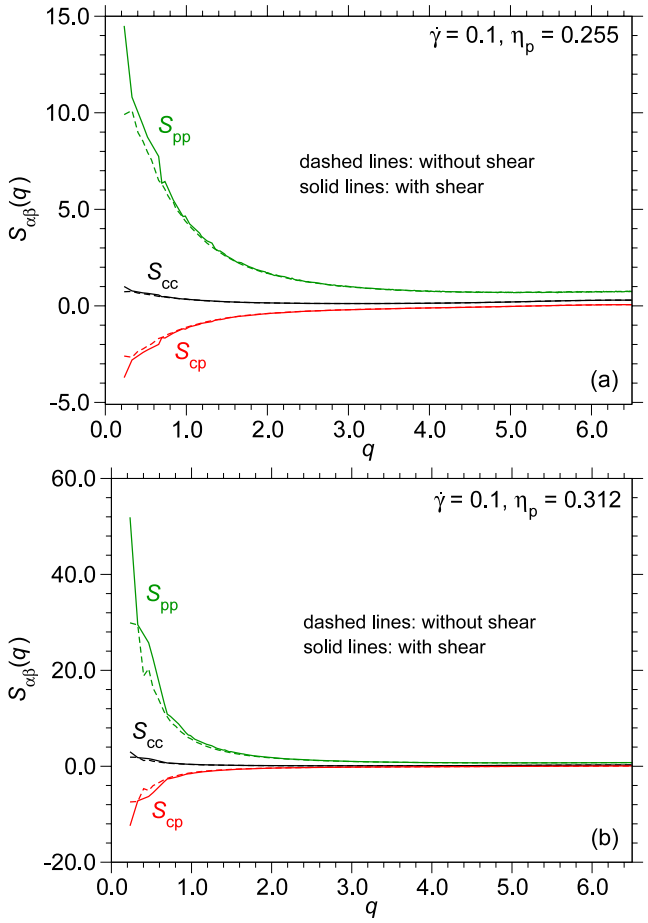

Figure 9. Partial static structure factors $S_{\alpha\beta}(q)$ plotted versus q for the system with box linear dimension $L = 27$, colloid packing fraction $\eta_c = 0.15$, shear rate $\dot{\gamma} = 0.1$ and two choices of the polymer packing fraction, $\eta_p = 0.255$ (a) and $\eta_p = 0.312$ (b). (This figure is in colour only in the electronic version)

$S_{\alpha\beta}(q)$, see figure 9. While some enhancement of $|S_{\alpha\beta}(q)|$ due to shear clearly is visible, unfortunately the statistical accuracy of the data does not warrant a quantitative analysis in terms of equation (23) yet. The necessary computational resources for a profound study of equation (23) were not available to us at this time. One can only see that for the smaller polymer packing fraction ($\eta_p = 0.255$ in figure 9(a)) there is only a small effect of shear rate, while for the larger polymer fraction ($\eta_p = 0.312$ in figure 9(b)) the effect is somewhat stronger.

As a final point, we consider the self-diffusion constants D_α of colloids ($\alpha = c$) and polymers ($\alpha = p$), as obtained from the mean-squared displacements perpendicular to the shear direction. Figure 10 shows the D_α as a function of η_p for the shear rate $\dot{\gamma} = 0.1$ in comparison to the unsheared case. It is interesting that under shear the D_α are slightly smaller. Moreover, D_p for the sheared case exhibits a shallow maximum around $\eta_p = 0.28$ and, for high values of η_p, it seems to decrease with increasing η_p, in contrast to the unsheared case. Also for this effect, a theoretical explanation is lacking. The behavior of various diffusion properties will be a subject of forthcoming studies. In particular, we aim at revealing the role of critical fluctuations in the anomalous behavior of D_p with and without shear.

6. Concluding remarks

In this paper, a soft version of the AO model for colloid–polymer mixtures, where polymers interact weakly (figure 1), has been presented and it was shown that the model is well suited for applications of MD simulation methods to study both equilibrium properties (static as well as time-displaced

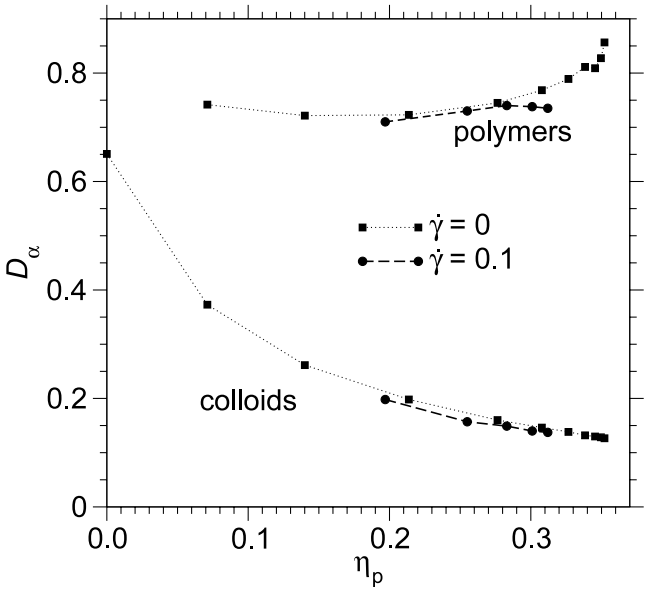

Figure 10. Self-diffusion constants of polymers and colloids for the unsheared system (open symbols) and the system under shear with shear rate $\dot\gamma = 0.1$ (closed symbols).

correlations) and properties under shear. The absence of interactions between the polymers in the ordinary AO model does not allow for a realistic modeling of dynamic properties. In particular, structural anisotropies of systems under shear are probably strongly underestimated by the ordinary AO model. The soft-repulsive interactions between the polymers in the modified AO model lead also to a slightly more realistic modeling of various static properties of the unsheared fluid (including the phase diagram).

While critical properties (static correlation length, susceptibilities, etc) in equilibrium are in accord with theoretical expectations at least roughly, the simulation data obtained in the present study cannot yet make a meaningful quantitative statement on the change of critical properties under shear. Our preliminary results (described in figures 7–10) show that some modification of properties due to shear can be identified, but the quality of the data does not yet suffice for a more precise test of the pertinent theory. However, we have shown how the correlation function $\mathrm{Im}g_{22}^{(\alpha\beta)(r)}$ ($\alpha\beta$ = cc, cp, pp) changes when approaching the critical point. In fact, this quantity is very useful to identify anisotropies in the critical fluctuations that are due to the application of shear. In forthcoming studies we shall extract the correlation length from $\mathrm{Im}g_{22}^{(\alpha\beta)}(r)$ which was not yet possible due to the lack of large computer resources.

In order to make further progress, it would also be desirable to extend the thermostat presented by Bussi *et al* [47] such that it is compatible with local momentum conservation, in order to respect hydrodynamics. Then large scale simulations with an efficiently parallelized version of the simulation code on a massively parallel computer would be needed to obtain simulation data with a very good statistical accuracy, and data at several shear rates as well as several colloid volume fractions need to be taken. Unfortunately, the huge computer resources necessary for such a study are yet unavailable. A conceptual problem is also that a viable method to identify the critical point in the presence of shear is needed. Thus, the simulation study of colloid–polymer mixtures under shear remains a challenging problem.

Acknowledgments

This work received financial support from the Deutsche Forschungsgemeinschaft, SFB TR6/A5. Computing time on the JUMP at the NIC Jülich is gratefully acknowledged. We thank M Parrinello for his hint to [47].

References

[1] Poon W C K 2002 *J. Phys.: Condens. Matter* **14** R859
[2] Poon W C K 2004 *Science* **304** 830
[3] Ilett S M, Orrock A, Poon W C K and Pusey P N 1995 *Phys. Rev.* E **51** 1344
[4] Likos C N 2001 *Phys. Rep.* **348** 267
[5] Löwen H 2001 *J. Phys.: Condens. Matter* **13** R415
[6] Löwen H and Likos C N (ed) 2004 Colloidal dispersions in external fields *J. Phys.: Condens. Matter* **16** (special issue)
[7] Asakura S and Oosawa F 1954 *J. Chem. Phys.* **22** 1255
[8] Asakura S and Oosawa F 1958 *J. Polym. Sci.* **33** 183
[9] Vrij A 1976 *Pure Appl. Chem.* **48** 471
[10] Van Blaaderen A 1997 *Prog. Colloid Polym. Sci.* **104** 59
[11] Aarts D G A L, Schmidt M and Lekkerkerker H N W 2004 *Science* **304** 847
[12] Wijting W K, Besseling N A M and Stuart M A C 2003 *Phys. Rev. Lett.* **90** 196101
[13] Aarts D G A L 2005 *J. Phys. Chem.* B **109** 7407
[14] Hennequin Y, Aarts D G A L, Indekeu J O, Lekkerkerker H N W and Bonn D 2008 *Phys. Rev. Lett.* **100** 178305
[15] Royall C P, Aarts D G A L and Tanaka H 2007 *Nat. Phys.* **3** 636
[16] Aarts D G A L and Lekkerkerker H N W 2004 *J. Phys.: Condens. Matter* **16** S4261
[17] Derks D, Aarts D G A L, Bonn D, Lekkerkerker H N W and Imhof A 2006 *Phys. Rev. Lett.* **97** 038301
[18] Dijkstra M, van Roij R, Roth R and Fortini A 2006 *Phys. Rev.* E **73** 041404
[19] Dijkstra M and van Roij R 2002 *Phys. Rev. Lett.* **89** 208303
[20] Vink R L C, Horbach J and Binder K 2005 *Phys. Rev.* E **71** 011401
[21] Vink R L C, Horbach J and Binder K 2005 *J. Chem. Phys.* **122** 134905
[22] Binder K, Horbach J, Vink R L C and De Virgiliis A 2008 *Soft Matter* **4** 1555
[23] Bolhuis P G, Louis A A, Hansen J-P and Meyer E J 2001 *J. Chem. Phys.* **114** 4296
[24] Bolhuis P G, Louis A A and Hansen J-P 2002 *Phys. Rev. Lett.* **89** 128302
[25] Bolhuis P G and Louis A A 2002 *Macromolecules* **35** 1860
[26] Louis A A 2002 *J. Phys.: Condens. Matter* **14** 9187
[27] Rotenberg R, Dzubiella J, Louis A A and Hansen J-P 2004 *Mol. Phys.* **102** 1
[28] Zausch J, Virnau P, Binder K, Horbach J and Vink R L C 2009 *J. Chem. Phys.* **130** 064906
[29] Hansen J P and McDonald I R 1986 *Theory of Simple Liquids* (San Diego, CA: Academic)
[30] Vink R L C and Horbach J 2004 *J. Chem. Phys.* **121** 3253
[31] Binder K 1997 *Rep. Prog. Phys.* **60** 487

[32] Landau D P and Binder K 2009 *A Guide to Monte Carlo Simulation in Statistical Physics* 3rd edn (Cambridge: Cambridge University Press)
[33] Allen M P and Tildesley D J 1987 *Computer Simulation of Liquids* (Oxford: Clarendon)
[34] Evans D J and Morris G P 1990 *Statistical Mechanics of Nonequilibrium Liquids* (London: Academic)
[35] De Gennes P G 1979 *Scaling Concepts in Polymer Physics* (Ithaca, NY: Cornell University Press)
[36] Vink R L C, Jusufi A, Dzubiella J and Likos C N 2005 *Phys. Rev.* E **72** 030401(R)
[37] Barker J A and Henderson J 1967 *J. Chem. Phys.* **47** 4714
[38] Das S K, Horbach J and Binder K 2003 *J. Chem. Phys.* **119** 1547
[39] Das S K, Horbach J, Binder K, Fisher M E and Binder K 2006 *J. Chem. Phys.* **125** 024506
[40] Bhatia A B and Thornton D E 1970 *Phys. Rev.* B **2** 3004
[41] Fisher M E 1968 *Phys. Rev.* **176** 257
[42] Binder K and Luijten E 2001 *Phys. Rep.* **344** 179
[43] Lees A W and Edwards S F 1972 *J. Phys. C: Solid State Phys.* **5** 1921
[44] Zausch J 2009 *Dynamics, Rheology and Critical Properties of Colloidal Fluid Mixtures: Molecular Dynamics Studies in Equilibrium and Under Shear* (Saarbrücken: Südwestdeutscher Verlag für Hochschulschriften)
[45] Hoogerbrugge P J and Koelman J M V A 1992 *Europhys. Lett.* **19** 155
[46] Peters E 2004 *Europhys. Lett.* **66** 311
[47] Bussi G, Donadio D and Parrinello M 2007 *J. Chem. Phys.* **126** 014101
[48] Berendsen H J C, Postma J P M, van Gunsteren W F, DiNola A and Haak J R 1984 *J. Chem. Phys.* **81** 3684
[49] Hanley H J M, Rainwater J C and Hess S 1987 *Phys. Rev.* A **36** 1795
[50] Onuki A and Kawasaki K 1979 *Ann. Phys.* **121** 456
[51] Beysens D and Gbadamassi M 1980 *Phys. Rev.* A **22** 250